Manganese incorporation in synthetic hercynite

Manganese incorporation in synthetic hercynite

G.D. Bromiley[1,2*]
G.D. Gatta[3,4]
T. Stokes[1]

1. School of GeoSciences, Grant Institute, University of Edinburgh, King's Buildings, Edinburgh EH9 3JW, UK.
2. Centre for Science at Extreme Conditions, Erskine Williamson Building, University of Edinburgh, King's Buildings, Edinburgh EH9 3JZ, UK.
3. Dipartimento di Scienze della Terra, Università degli Studi Milano, Via Botticelli 23, I-20133 Milano, Italy.
4. CNR - Istituto di Cristallografia, Sede di Bari, Via G. Amendola 122/o, I-70126 Bari, Italy

*Email: geoffrey.bromiley@ed.ac.uk

Abstract

Manganese incorporation in synthetic hercynite, and partitioning between hercynite and silicate melt synthesised at 1.0 GPa, 1250°C, and at a fO_2 buffered by Fe-FeO, has been studied by X-ray absorption spectroscopy and single-crystal X-ray structure refinement. Spectra indicate the presence of both Mn^{2+} and Mn^{3+} (and possibly also Mn^{4+}) in synthetic hercynite and partitioning of Mn^{2+} into the melt phase, and Mn^{3+} into hercynite, respectively, under run conditions. X-ray refinement is consistent with partial disorder of Fe and Al across tetrahedral and octahedral sites. A higher than expected degree of Fe-Al disorder in the Mn-bearing hercynite can be explained by preferential incorporation of Mn^{2+} onto the tetrahedral site, and indicates that Fe-Al disorder in pure, stoichiometric hercynite cannot necessarily be used to determine closure temperatures in natural spinel. However, partitioning of Mn^{2+} and Mn^{3+} between melt and hercynite suggests that Mn incorporation in hercynite could be used as a measure of fO_2 conditions in magmas during spinel crystallisation.

Running title: Mn incorporation in hercynite

Key words: hercynite, spinel, manganese, oxygen fugacity, disorder, crystal chemistry

Introduction

Spinel group minerals ('spinels') with the general formula AB_2O_4 are common within Earth's crust and mantle and are important industrial and technological materials. This is in part due to the ability of the spinel structure to accept a wide variety of elements, including transition metals such as Fe, Mo, Zn, Mn, Ti, Cr and V. As a consequence, naturally occurring spinels are typically complex solid solutions involving a large number of components. Hercynite, $Fe^{2+}Al_2O_4$, is one such component and occurs in significant concentrations in spinels in a range of geological settings, from metamorphosed iron-rich argillaceous sediments to mafic and ultramafic igneous rocks (Anthony *et al.*, 1997). A complete solid solution exists between hercynite and spinel sensu stricto (s.s.), $MgAl_2O_4$ (Turnock and Eugster, 1962). Complete solid solution between hercynite and magnetite, $Fe^{2+}Fe^{3+}{}_2O_4$, is also noted at high temperatures, and as a result, Al-bearing spinels, including those enriched in hercynite component, are stable over a wide range of pressure-temperature (*P*-*T*) and oxygen fugacity (fO_2) conditions within the Earth (Woodland and Wood, 1990; Schollenbruch *et al.*, 2010).

Minerals such as hercynite and spinel s.s. are commonly referred to as 2-3 spinels. In the spinel structure, oxygen atoms form a dense, approximately cubic-close-packed arrangement, with cations present in tetrahedral (*T*) or octahedral (*M*) coordination. In an ideal model, 2-3 spinel structure divalent A cations are present on tetrahedral sites and trivalent B cations on octahedral sites, the presence of two octahedral and one tetrahedral site per formula unit thereby giving rise to the ideal

AB_2O_4 formula. However, spinel group minerals are typically characterised by varying degrees of cation disorder on the *M* and *T* sites, and as such the general formula is more accurately expressed as:

$$A_{1-x}B_x\left(A_{\frac{x}{2}}B_{1-\left(\frac{x}{2}\right)}\right)_2O_4$$

where the variable *x* is described as the 'inversion parameter' (Harrison *et al.*, 1998). In this scheme, two ordered configurations of 2-3 spinels are possible, with *x* = 0 for the normal configuration and *x* = 1 for an 'inverse' configuration. Hercynite and spinel s.s. are 'normal' spinels, with values of *x* close to 0, although at elevated temperature the cations become increasingly randomly distributed over *T* and *M* sites (Harrison *et al.*, 1998; Redfern *et al.*, 1999). A value of *x* = 2/3 corresponds to a completely disordered spinel structure. The order-disorder process in spinels is non-convergent and involves no change in symmetry. Naturally occurring spinels are predominantly cubic ($Fd\bar{3}m$ space group), with a single O atom at *u,u,u,* fractional coordinates and *M* and *T* cations at fixed positions. Modification of *T-O* and *M-O* bond distances to accommodate various chemical substitutions and cation disordering results in variations in the *O* positional coordinates and the cubic cell edge length (Andreozzi and Lucchesi, 2002).

The ability of spinel-group minerals to incorporate multi-valent transition metals such as Fe, Mn and V, and measurements of cation disorder to independently determine closure temperature (Harrison *et al.*, 1998; Redfern *et al.*, 1999), means that naturally occurring spinels can potentially be used as a probe of the oxidation state of magma from which host rocks crystallised. The stability of Fe-

rich end-member spinels as a function of fO_2 has been extensively studied (see below). Magnetite is stable over a range of approximately 5 log units of fO_2, defined by its breakdown at reducing conditions to wustite (FeO), which marks the reduction of ferric iron, and at more oxidising conditions by oxidation of ferrous iron and formation of hematite (Fe_2O_3). In fact, the well characterised magnetite-wustite and magnetite-hematite reactions are commonly used as redox buffers in experimental studies, or as references for comparing measured fO_2 conditions (e.g., Myers and Eugster, 1983). In air and at atmospheric pressure, magnetite oxidises rapidly to maghemite, γ-Fe_2O_3, one of the few naturally occurring spinels which contains high concentrations of cation vacancies (e.g., Johnson and Jensen, 1974). The stability of magnetite over a range of conditions found within the deep Earth and its incorporation of mixed-valent Fe means that reactions between olivine, orthopyroxene and spinel can be used to determine prevalent fO_2 conditions in spinel-bearing mantle peridotites (for example see Raye *et al.,* 2011, and references therein). There have been numerous studies of other Fe-bearing spinels under varying fO_2 conditions, although the majority of these are within the fields of material science and solid state chemistry due to their importance in a wealth of applications from high-density magnetic recording media to reduction catalysts. Recently, Liang et al (2013) studied the thermal stability of magnetite substituted with varying amounts of Ti, Mn, Co, Ni, V and Cr. Although their study focussed on the influence of dopants on high-temperature stability, it does provide useful insight into the substitution mechanisms for multi-valent cations into Fe-rich spinels. Lavina *et al.* (2005) studied progressive oxidation of Mg-hercynite during heating and documented systematic variations in Fe^{2+}/Fe^{3+} ratios and cation vacancy contents. Woodland and Wood (1990) determined the stability of hercynite under reducing

conditions, and noted that Fe-bearing natural hercynite could potentially be used as a monitor of fO_2 in rocks. Halenius *et al.* (2002) used optical and Mössbauer spectroscopy to investigate Fe^{3+} incorporation in a series of synthetic hercynitic spinels. The proportion of Fe^{3+} in Fe-rich synthetic spinel appears, as expected, to depend partly on fO_2 conditions used during synthesis, with studies by Lenaz et al. (2004, 2006) showing high to negligible Fe^{3+} contents in synthetic spinels depending on synthesis conditions and starting materials used. Halenius *et al.* (2002) report that Fe^{3+} is strongly ordered onto the *M* site in hercynite, consistent with the normal ordering of this spinel and with studies of other natural and synthetic spinels (e.g., Carbonin, 1996; Lenaz *et al*., 2002, 2006). In one of the few systematic studies of the influence of redox conditions on multivalent cation incorporation in natural spinels, Righter *et al.* (2006) studied the influence of fO_2 on V incorporation in synthetic spinels and on spinel-melt partitioning, and noted systematic variations in the proportions of V^{3+}, V^{4+} and V^{5+} with decreasing fO_2.

Despite these studies, the potential for spinel-group minerals as indicators of fO_2 conditions within rocks independent of mineral equilibria remains relatively untested. In particular, few studies have focussed on the oxidation state and distribution of multi-valent cations within spinel structures under deep Earth conditions. Aside from Fe and V, Mn is also a multivalent element worthy of consideration. Under terrestrial conditions it can exist in 2+, 3+, 4+ and possibly 5+ oxidation states, is the 12th most abundant element in the Earth's crust and can readily substitute into the spinel structure. Manganese iron spinels $(Mn_xFe_{1-x})_3O_4$ have been extensively studied due to potential applications as magnetic recording media and in electronic devices. For Mn contents below $x = 0.6$, these spinels are cubic. Variation in structural and magnetic properties with preparation conditions

suggest complex relationships between cation valence and ordering with fO_2 and temperature (Guillemet-Fritsch *et al.*, 2005). Beard and Tracy (2002) studied the metamorphosed Mn-rich magnetite from the Hutter Mine locality, and detailed solid solutions between the spinels magnetite, jacobsite $(Mn^{2+},Fe^{2+})(Mn^{3+},Fe^{3+})_2O_4$ and galaxite ($MnAl_2O_4$). Galaxite is a normal spinel, in contrast to magnetite and jacobsite which are inverse. Beard and Tracey (2002) noted substantial solid solution between jacobsite and galaxite, consistent with structural data on the end-member species and a marked preference of Mn(2+) for the *T* site in the spinel structure. Lucchesi et al. (1997) studied the crystal chemistry of natural Mn-rich spinels directly and confirmed that Mn^{2+} shows a strong preference for the *T* site in Mn-rich spinels, resulting in increased preference of Fe^{3+} for the *M* site. Although not confirmed by X-ray refinements, they also noted stoichiometric evidence for the presence of some Mn^{3+} in the same samples. Lucchesi *et al.* (1997) note that this is consistent with a number of previous experimental and theoretical studies which show evidence for strong partitioning of Mn^{2+} onto *T* sites and Mn^{3+} onto *M* sites in the spinel structure (e.g., O'Neill and Navrotsky, 1983). In contrast, Bosi et al. (2007) demonstrated that spinels synthesised along the $MgAl_2O_4$-$MgMn_2O_4$ join, using a flux-growth method, contain increasing proportions of octahedral Mn^{2+} and increasing proportions of tetrahedral Mn^{3+} with increasing Mn content, although presumably this high degree of disorder is partly a function of the high temperatures of synthesis, and it is uncertain whether results can easily be applied to natural spinels which characteristically have low Mn contents.

Determining Mn oxidation state in spinels is complicated by the presence of multivalent iron, due to the observed equilibrium (Lotgering, 1964):

$$Mn^{2+} + Fe^{3+} = Mn^{3+} + Fe^{2+} \quad [1]$$

although the presence of this redox reaction further highlights the potential for Mn-Fe bearing spinels to record inherent redox conditions. There are, however, relatively few studies of Mn incorporation using methods which accurately distinguish oxidation state, especially in natural samples or in non-endmember compositions. Previous studies clearly highlight that Mn can be incorporated into spinel in at least 2 oxidation states, and distributed to varying degrees over both cation sites. However, the degree to which this occurs in natural spinels under terrestrial conditions, especially at elevated pressure where defect spinels are unstable, remains uncertain. Here, as part of a systematic study of Mn oxidation state in Earth materials, we use single crystal X-ray diffraction (XRD), X-ray Absorption Near-Edge Structure spectroscopy (XANES) and electron probe microanalysis in wavelength dispersive mode (EMPA) to study the crystal chemistry of Mn-bearing hercynite grown in an analogue natural composition under high pressure-temperature conditions.

Sample synthesis and chemical characterisation

Natural analogue hercynite in equilibrium with Fe-rich silicate glass was synthesised at 1.0 GPa using an end-loaded piston-cylinder apparatus. Starting materials were prepared from finely ground natural granite from the Criffell pluton in Scotland (sample AM09.17 from Miles *et al.* (2013)) to which was added 30wt% of an oxide mix of ideal apatite composition $Ca_5(PO_4)_3OH$, and 5 wt% MnO_2. This mixture was homogenised by grinding under high-purity acetone, dried and loaded into a Pt foil lined high-purity, 4mm outer diameter Fe capsule. Details of the capsule design,

which effectively buffers fO_2 at the Fe-FeO (IW) buffer is given in Bromiley *et al.* (2004). Reaction of the capsule with the experimental charge ensured Fe saturation in the melt during the experiment, thereby stabilising hercynite. However, by acting as a source for reduced Fe which diffuses into the experimental charge, this capsule design also ensures that fO_2 conditions inhibited Fe oxidation and enrichment of the sample in Fe^{3+}. The capsule, with press-fit lid to prevent volatile release during the experiment, was loaded into a machined alumina sleeve and inserted into a 0.5" talc-pyrex-graphite assembly, as described in Bromiley *et al.* (2010). The experiment was run using the hot-piston out technique by pressurising to 120% of the final run pressure, heating to 1450°C at a rate of 100°C/minute whilst maintaining pressure, and then slowly bleeding off oil until the desired run pressure was attained. Temperature was monitored throughout using a Pt-Pt13%Rh thermocouple adjacent to the capsule (for full details including calibration see Bromiley *et al.*, 2010). At 1450°C, this bulk composition is expected to be above the liquidus. After 1 hour, temperature was slowly ramped down to 1250 °C at a rate of 5°C/minute, whilst maintaining run pressure, to promote growth of large crystals. Temperature was then maintained at 1250 °C for an additional 24 hours before the run was quenched and recovered. The run was quenched by switching off power to the heating circuit which resulted in temperature falling from 1250 °C to less than 150 °C within 10 s. The recovered capsule was embedded in epoxy and ground and polished to reveal a longitudinal section. Visual examination of the polished sample in reflected light revealed the presence of a two phase mixture of well-formed trapezoidal crystals up to 125μm diameter within a matrix of quenched glass free of any crystallites. Compositions of mineral and quenched glass were then determined using a Cameca SX-100 microprobe in wavelength dispersive mode. Crystal compositions were

determined using a 15 kV accelerating voltage and 20 nA beam current, with a 5μm beam diameter. For analysis of crystals the following standards, analysing crystals and count times were used for each successive element: Ca (synthetic Ca-spinel, PET, 20s), Na (jadeite, LTAP, 20s), K (orthoclase, PET, 20s), Sr (celestite, PET, 30s), Mn (Mn metal, LLIF, 40s), Mg (spinel, LTAP, 40s), Fe (fayalite, LLIF, 40s), Al (spinel, TAP, 20s), Si (wollastonite, TAP, 20s). *K*α lines for all elements were used except for Sr, for which the *L*α line was used. Glass compositions were determined using a 15 kV accelerating voltage and 2 nA beam current, again with a 5μm beam diameter. The following standards were used: Na (jadeite, LTAP, 20s), Mg (spinel, LTAP, 20s), Fe (fayalite, LLIF, 30s), Al (spinel, TAP, 20s), Si (wollastonite, TAP, 20s), K (orthoclase, PET, 20s), Ca (wollastonite, PET, 20s), Cl (NaCl, PET, 20s), P (synthetic P-rich spinel, PET, 20s), S (barite, PET, 20s), Ti (rutile, PET, 20s), F ($RbMnF_3$ spinel, TAP, 60s). *K*α lines were used for all analyses. PAP mins and XPHI correction procedures were applied using the in-built Cameca "Peak Site" v5 analysis software. Multiple point analysis of glass (8 analyses) revealed a uniform silicate composition, and multiple point analyses of the crystalline phase (10 analyses) revealed that these had a uniform, Mn-bearing hercynitic composition (Table 1). Transects across larger crystals also revealed that they had uniform compositions and were not zoned. Averaged analyses from point analyses for hercynite and glass are listed in Table 1.

X-ray absorption spectroscopy

Microfocus Mn *K*-edge XANES spectra from the synthetic hercynite crystals and coexisting glass and from a series of standards were collected on beamline I18 at

the Diamond Light Source (DLS), Harwell, UK. Data were collected in fluorescence geometry with polished, epoxy-mounted samples at 45° to the incident X-ray beam. A Si(111) double crystal monochromator was used to tune the energy of the beam which was focussed onto the sample to produce a beam spot size of approximately 6µm x 6µm. Fluorescing X-rays from the sample were detected using a Ge XSPRESS detector, and Mn foil was used to calibrate the energy of the Mn edge, with an uncertainty in energy of ±0.05 eV. For most samples, a 0.1mm Al foil sheet was placed in front of the detector to screen out lower energy absorption peaks. Pre-edge data were collected at 5eV steps with a 0.5 s scanning time whereas pre-edge peak and main absorption peaks were collected at 0.5 eV steps and 0.5 s scanning time. Repetitive scans were taken to assess radiation damage, although we found no evidence (e.g., reduction of Mn) on samples even when repetitive scans were taken on the same spot. Processing and Linear Combination Fitting (LCF) of hercynite and glass XANES spectra was performed using built-in functions in the ATHENA software (Ravel and Newville, 2005). The AUTOBK algorithm was used to model and remove the background using a spline-fit procedure, following normalisation and deglitching. Comparison of this procedure with the method outlined by Manceau et al. (2012) for several different spectra demonstrated that it led to comparable background subtracted spectra. A series of spectra from reference single valence Mn materials collected as part of this study (i.e., pyrolusite, bixbyite, manganite and rhodonite, provided by the Cockburn Geological Museum, University of Edinburgh) and published spectra from Manceau et al. (2012) (i.e., pyrolusite, ramsdellite, $Ca_2Mn_3O_8$, KBi, groutite, feitknechtite, manganite, Mn_2O_3, $MnPO_4$, hureaulite, Mn-sorbed fungi, rhodocrosite, manganosite, pyroxmangite, tephroite and Mn aqueous solutions) were used for LCF. Fitting was applied to first-derivative spectra using all

available standards simultaneously (as outlined in detail in Manceau *et al.*, 2012), and the combination of standards which gave the best fit in terms of *R* factor determined for each spectrum. All fits were then compiled from the whole data set to determine average valences of Mn^{2+}, Mn^{3+} and Mn^{4+} (Table 2).

Single-crystal XRD

A crystal of hercynite-Mn (0.15 x 0.13 x 0.09 mm^3) was selected from the sectioned capsule for the single-crystal X-ray diffraction experiment. Intensity data were collected at room conditions using an Oxford Diffraction Xcalibur diffractometer, equipped with a CCD detector and operating at 50 kV and 40 mA with monochromatized Mo*K*α radiation. A combination of ω scans, with 1° step and 20 s exposure time per frame, was chosen to maximize the redundancy and data coverage. A total number of 3527 Bragg reflections were collected, with a $2\theta_{max}$ = 71.5°, out of which 84 were unique for symmetry. Least-squares refinement of the peak positions leads to the following unit-cell constant: *a* = 8.1646(2) Å. The reflection conditions agreed with the space group $Fd\bar{3}m$. Intensity data were integrated and corrected for Lorentz-polarization and absorption effects (by Gaussian integration based upon the physical description of the crystal) using the CrysAlis software package (Agilent, 2012). After these corrections, the discrepancy factor between symmetry-related diffraction intensities (Laue class *m*3*m*) was R_{int} = 0.0247 (Table 1).

The anisotropic structural refinement of the Mn-bearing hercynite was performed using the SHELX-97 software (Sheldrick, 1997) starting from the atomic coordinates of Harrison *et al.* (1998). Neutral atomic scattering factors for O, Al, Mn

and Fe were taken from the *International Tables for Crystallography (Wilson and Prince, 1999)*. Secondary isotropic extinction effects were corrected according to the formalism of Larson (1967), as implemented in the SHELXL-97 package (Sheldrick, 1997). Two structure refinements were performed as discussed below.

Results and Discussion

Mn valence and incorporation

Electron microprobe data for the synthetic spinel phase (Table 1) are consistent with a Mn-bearing hercynite-rich spinel formula of composition $(Fe_{0.84}Mg_{0.05}Mn_{0.15}Si_{0.02}Al_{1.92})O_4$, based on the assumption that all Fe present in the synthetic hercynite is Fe^{2+}. This is consistent with the run conditions used which maintain an inherently low fO_2 and the use of an Fe capsule as a source of reduced Fe to minimize the presence of Fe^{3+} in the run products. There have, however, been several reports of Fe^{3+} defects in synthetic hercynite, so in the absence of a direct determination of Fe oxidation state, consideration of the stability of Fe^{3+} defects in spinel is warranted. Halenius *et al.* (2002) synthesized hercynitic spinels and spinel solid solutions using a flux-growth method in a gas-mixing apparatus with a CO_2-H_2 gas mix chosen to produce reducing conditions, and demonstrated the presence of Fe^{3+} defects using optical and Mössbauer spectroscopy and results from previously published single crystal X-ray diffraction. Whilst noting that the proportion of Fe^{3+}/total Fe was markedly reduced at lower fO_2, Halenius *et al.* (2002) observed that some Fe^{3+} was present in samples synthesized at the most reducing conditions used, close to the IW buffer. Similarly, the presence of variable quantities of Fe^{3+} in synthetic spinels has also been reported by Andreozzi *et al.* (2001), Lavina *et al.* (2005) and Lenaz *et al.* (2006). In contrast, other studies report that hercynite

synthesized under more reducing conditions contains negligible Fe^{3+} (e.g., Harrison *et al*., 1998; Lenaz *et al*., 2004). Careful examination of synthesis conditions used in these studies suggests that 2 factors are likely to explain oxidation of Fe in hercynite. Halenius *et al.* (2002) note that during synthesis runs they controlled fO_2 using a fixed ratio gas mix designed to buffer fO_2 close to IW. They then ramped run temperatures down from 1200 to 900°C to promote crystal growth whilst maintaining the gas mix, which would have slightly reduced fO_2. However, the temperature dependence of fO_2 imparted by a CO_2-H_2 gas mix differs from that of the IW buffer, such that reduction in run temperature would have raised fO_2 relative to IW. More importantly, Halenius *et al.* (2002) then terminated runs by allowing samples to cool within the furnace apparatus used, rather than attempting to rapidly quench run products. Subsequent sample cooling rates in their study are not given and are difficult to ascertain, although experience suggests that they could be considerable and that rapid (drop) quenching is required to prevent partial oxidation of samples during cooling. Cooling of samples in a fixed gas mix would result in sample oxidation relative to the IW buffer and would likely result in partial oxidation of Fe^{2+} to Fe^{3+}. For example, at 600°C, the 2 main gas mixes used by Halenius *et al.* (2002) lie considerably above the IW buffer, and probably even above the magnetite-FeO (MW) buffer (Myers and Eugster, 1983) depending on instrument calibration. Other studies in which substantial Fe^{3+} defects in hercynitic spinels are reported use either a similar synthesis technique in which fO_2 cannot be considered to be effectively buffered relative to Fe redox reactions, or involve synthesis under much more oxidizing conditions, sometimes even in air, and/or from starting mixes enriched in Fe^{3+} (e.g., Andreozzi *et al.,* 2001; Lenaz *et al.,* 2006; Waerenborgh *et al.,* 1994). In

studies where reducing conditions are maintained and samples rapidly quenched (e.g., Harrison et al., 1998), there is no evidence for the presence of Fe^{3+}.

A second factor which may result in stabilization of Fe^{3+} defects in hercynite is stoichiometry of the *M* site. Halenius *et al.* (2002) note that their synthetic spinels are Al-deficient, and consider this as a factor in stabilizing Fe^{3+} defects which are then strongly ordered onto the *M* site. Furthermore, flux-growth of spinels at ambient pressure can also result in non-stoichiometry due to the presence of cation vacancies (see Bromiley *et al*., 2010, and references therein) which might also conceivably stabilize defects such Fe^{3+}.

In the present study, we maintained reducing conditions throughout using a Fe-based capsule design and rapidly quenched samples to prevent later oxidation of Fe. The presence of an internal IW buffer means that fO_2 relative to the IW buffer could be verified from examination of run products. The use of an Fe capsule as an Fe source during the experiment also ensured that the sample is saturated in reduced Fe, further reducing the likelihood that Fe^{3+} defects could form. Furthermore, EMPA demonstrates that our hercynite sample is not Al-deficient but is instead slightly Fe-deficient relative to the stoichiometric formula for pure hercynite, and that full site occupancy can be assumed based on the presence of Fe^{2+}, Al and Mn without needing to invoke the presence of octahedral Fe^{3+}. Notable, the presence of cation vacancies in spinel is also inhibited by pressure, so in contrast to synthetic spinel samples grown using flux methods, which are characteristically non-stoichiometric and may contain high concentrations of cation vacancies and other defects (Bromiley *et al.,* 2010), samples synthesised here will not contain significant quantities of cation vacancies. Because we cannot verify that all Fe is present as

Fe^{2+}, we will also consider the possible influence of Fe^{3+} on hercynite crystal chemistry below.

Manceau et al. (2012) demonstrated that *K*-edge XANES data can be used to identify and determine Mn valence in Mn-bearing minerals due to clear and systematic shifts in absorption edge features (Manceau *et al.*, 2012). XANES spectra for standards with single valence Mn show a corresponding shift in near edge features (Figure 1). XANES spectra for synthetic hercynite and glass are clearly more complex than those obtained from single valence Mn-bearing reference minerals and are consistent with the presence of Mn in multiple oxidation states (Figure 2). Obvious differences between the spectra indicate that the glass contains a higher proportion of Mn^{2+} compared to hercynite, even though both phases were equilibrated under identical fO_2 conditions. Manceau *et al.* (2012) note that fitting of multi-valence Mn XANES spectra through use of single valence standards can result in an accuracy of approximately ±0.02 valence units (v.u.) although also note that accuracy of their fitting procedure is reduced for samples with higher proportions of Mn^{2+}, as is the case here. Results of the LCF procedure are listed in Table 2. The LCF procedure uses single valence Mn-bearing samples to fit sample spectra. Although a range of references were used, no suitable single valence reference could be found for Mn^{2+} in tetrahedral coordination (the only reported instances being in phases in which Mn can exist in multiple oxidation states and on multiple sites). As hercynite is expected to contain a significant proportion of tetrahedrally coordinated Mn^{2+}, the lack of a suitable reference limits the accuracy of the LCF procedure used. Despite this, reasonable fits were found for a combination of 2+ and 3+ for glass and 2+, 3+ and possibly 4+ for hercynite using the LCF procedure outlined by Manceau *et al.* (2012) and a full range of standards. However, the

complexity in near-edge features and the potentially low concentrations of Mn^{4+},make the presence of Mn^{4+} in hercynite spectra difficult to conclusively demonstrate. In accordance with Manceau *et al.* (2012), we note that the accuracy of fitting hercynite and glass spectra is reduced due to the presence of significant quantities of Mn^{2+} and estimate that the error in the LCF procedure used is of the order of 15-20% at best. However, we note that differences between hercynite and glass spectra and the presence of Mn in at least 2 oxidation states are obvious (even by visual examination of XANES data). Previous studies note that Mn^{2+} shows a strong preference for tetrahedral sites in spinel structures (Lucchesi *et al.*, 1997; Liang *et al.*, 2013) allowing the formula of the synthetic hercynite of this study to be rewritten as:

$^{T}(Fe_{0.84-x}Al_xMg_{0.05}Mn^{2+}_{0.07}Si_{0.02})^{M}(Fe_{x/2}Al_{0.96-x/2}Mn^{3+}_{0.04})_2O_4$ (not considering small quantities of Mn^{4+} present and the presence of any Fe^{3+}). Partitioning of Mn of different oxidation states between hercynite and glass within the experimental charge gives the following hercynite/melt partition coefficients: $D^{Mn2+}_{min/melt}$ = 0.57 (±0.1), $D^{Mn3+}_{min/melt}$ = 1.89 (±0.4) compared to an averaged Mn partitioning value of $D^{Mn}_{min/melt}$ = 0.9 (±0.06) based on EMPA. XANES data indicate, as expected under run conditions, that 2+ and 3+ oxidation states were stable in both hercynite and glass. Kohn *et al.* (1990) noted that modelling of XANES data on Mn incorporation in silicate melts indicated that Mn was dominantly 2+ and octahedrally coordinated. Preferential partitioning of Mn^{2+} into the melt phase over hercynite may, therefore, indicate a preference for Mn^{2+} to be octahedrally coordinated in the melt phase, as opposed to tetrahedrally coordinated in the spinel structure. There is clearly also a strong preference for Mn^{3+} to be both octahedrally coordinated and to enter hercynite over silicate melt. This is not surprising, as the vast majority of Mn-bearing minerals

contain Mn^{3+} in octahedral coordination. Mn was added to the starting material as MnO_2 (i.e., as Mn^{4+}), implying that the reducing conditions imparted by the capsule have reduced Mn significantly. However, the presence of appreciable quantities of Mn^{3+} suggests that either there is a significant crystal chemical control of Mn oxidation state and Mn incorporation, both for hercynite and to a lesser extent, silicate glass, and/or that partial oxidation of Mn^{2+} to Mn^{3+} occurred due to reaction [1].

Structure refinement of synthetic Mn-bearing hercynite

Two structure refinements were performed based on single-crystal X-ray data to determine the extent of Fe-Al disorder using the following protocols:

1) A first test refinement was performed using a mixed Al/Fe-scattering curve at the octahedral (*M*) and tetrahedral (*T*) sites. The fraction of Al and Fe at the *M* and *T* sites were refined. No other element was considered to model the cationic population. Convergence was rapidly achieved and the variance–covariance matrix did not show any significant correlation between the refined parameters. At the end of refinement, the residuals in the difference-Fourier maps of the electron density were less than ±0.3 $e^-/Å^3$, with an agreement factor $R_1(F)$ = 0.0115 based on 79 unique reflections with $F_O > 4\sigma(F_O)$ and 10 refined parameters (Table 3). Atomic positions, site occupancy factors (s.o.f.), displacement parameters and bond distances are also reported in Table 3.

2) A second refinement was performed based on the composition of hercynite determined from EMPA (not including minor amounts of Mg and Si), and with a Mn distribution across cations sites in accordance with XANES data. Fixed fractions of Mn of 0.07 a.p.f.u. at the *T* site and 0.04 a.p.f.u. at the *M* site were used, consistent with an approximate 0.45:0.55 distribution of Mn^{2+} and Mn^{3+} and based on the assumption that Mn^{2+} preferentially partitions onto the *T* site in spinels, and Mn^{3+} onto the *M* site (Lucchesi *et al.*, 1997). Mixed Al/Fe-scattering curves were used to model the remaining cationic population at the octahedral and tetrahedral sites, and the fractions of Al and Fe were refined. With this configuration, convergence was rapidly achieved without any significant correlation between the refined parameters. At the end of refinement, the residuals in the difference-Fourier maps were less than ±0.3 $e^-/Å^3$, with an agreement factor $R_1(F)$ = 0.0114 based on 79 unique reflections with $F_O>4\sigma(F_O)$ and 10 refined parameters (Table 3). Atomic positions, site occupancy factors, displacement parameters and bond distances are also reported in Table 3.

Fe-Al disorder in Mn-bearing hercynite

The single-crystal X-ray diffraction data show that the unit-cell constant of our Mn-hercynite is *a* = 8.1646(2) Å, with *u* parameter equal to 0.26375(9). In spinels, the length of the cell edge is geometrically related to the polyhedral bond distances, which in turn reflect the degree of ordering. Using a mixed Al/Fe scattering curve to model the *T* and *M* sites (refinement protocol 1), we obtained: $^{T}(Fe_{0.84(1)}Al_{0.16(1)})$ and $^{M}(Al_{0.838(5)}Fe_{0.162(5)})$. The structure refinement with the fraction of Mn fixed at the *T* and *M* sites on basis of the EMPA and XANES data (refinement protocol 2) led to:

$^{T}(Fe_{0.77(1)}Al_{0.16(1)}Mn_{0.07})$ and $^{M}(Al_{0.834(5)}Fe_{0.126(5)}Mn_{0.040})$, with a resulting 1.02(2) a.p.f.u. of Fe, 1.83(2) a.p.f.u. of Al and 0.15 a.p.f.u. of Mn. The multi-element population in our hercynite at the *T* and *M* sites, deduced on the basis of the chemical analysis, makes the refined Al/Fe-fractions of the structure refinements only "virtual". In this light, we did not apply any restraint on the inter-site distribution of Al and Fe (*e.g.*, s.o.f.^{M}(Fe) = 1- 0.5·s.o.f.^{T}(Al)), as usually done for the ideal hercynite (*e.g*. Harrison *et al.*, 1998). The "actual" result provided by the structure refinements is the refined electron content per site: for the Mn-free refinement we obtain a Σe- = ^{T}(23.92) + ^{M}(15.11) = 39.03 *e*- and for the refinement in which Mn is included Σe- = ^{T}(23.85) + ^{M}(15.12) = 38.97 *e*-, two almost identical values. The refined electron contents per site (*i.e*., ~23.9 at the *T* site and ~15.1 at the *M* site) reflect a degree of inter-site Al/Fe-disorder. The calculated sum of the electron content at the *T* and *M* sites on the basis of the multi-element distribution obtained by EMPA and XANES data led to Σe- = 38.47 *e*-, in good agreement with the data obtained by the X-ray structure refinements. The structure refinements converged with displacement parameters of the tetrahedral, octahedral and oxygen sites with: $U_{eq}(T):U_{eq}(M):U_{eq}(O) \approx 1.1:1:1.51$. This scheme agrees with the previous experimental findings on hercynite at room conditions (*e.g*., Hill, 1984; Larsson *et al.*, 1994; Harrison *et al.*, 1998; Lavina *et al.*, 2005, 2009).

Harrison *et al.* (1998) reported a cell constant of 8.14578(3) Å for synthetic hercynite ($FeAl_2O_4$) by neutron powder diffraction at room conditions, with refined Fe/Al-fractions of $^{T}(Fe_{0.865(4)}Al_{0.135(4)})$ and $^{M}(Al_{0.933(2)}Fe_{0.067(2)})$. A unit-cell edge of ~8.169 Å (*i.e*., similar to that observed in our study) was measured by Harrison *et al.* (1998) at higher temperature, ~670 K, although with a virtually identical ordering scheme as that obtained at 298 K: $^{T}(Fe_{0.866(4)}Al_{0.134(4)})$ and $^{M}(Al_{0.933(2)}Fe_{0.067(2)})$.

Andreozzi and Lucchesi (2002) similarly reported the structure refinement of a synthetic hercynite with unit-cell constant of ~8.165 Å (*i.e.*, virtually identical to that observed in our study), with the following ordering scheme: $^{T}(Fe^{2+}_{0.85(2)}Fe^{3+}_{0.02(2)}Al_{0.13(2)})$ and $^{M}(Al_{0.88(1)}Fe^{2+}_{0.08(1)}Fe^{3+}_{0.04(1)})$. Therefore, previous experimental findings suggest that in chemically ideal hercynite, a unit-cell edge of ~8.165 reflects Fe/Al-disordering between *T* and *M* sites, in agreement with the experimental results of this study.

Geological implications of Mn incorporation in hercynite

EMPA, XANES and X-ray structure refinement of the synthetic hercynite of this study are consistent with partial Fe-Al disorder, a non-stoichiometric Fe:Al, presence of Mn^{2+} and Mn^{3+} partitioned over *T* and *M* sites respectively, and the presence of minor additional cations. This can be expressed in the following chemical formula: $^{T}(Fe_{0.77(1)}Al_{0.09(3)}Mg_{0.05(1)}Mn^{2+}_{0.07(2)}Si_{0.02(1)})^{M}(Fe_{0.126(6)}Al_{0.834(5)}Mn^{3+}_{0.04(1)})_2O_4$, with errors derived by structure refinement, fitting XANES spectra and EMPA. Occupancy of Mg and Si have not been determined in the structure refinement and are simply assigned to the *T* site. The (virtual) refined fraction of Al at the tetrahedral site (i.e., 0.16(1), Table 3) actually represents the co-presence of Al, Mg and Si; on this basis, we can deduce that ^{T}(Al + Mg + Si) = 0.16(1) a.p.f.u. (Table 3) and, combining the EMPA data of Mg and Si (i.e., $Mg_{0.05(1)}$ and $Si_{0.02(1)}$ a.p.f.u.), we obtain: ^{T}Al = 0.09(3) a.p.f.u.. Within error, this represents a balanced spinel formula with no evidence for cation vacancies. The extent of Fe-Al site mixing in our synthetic hercynite cannot be directly compared with data from Harrison et al. (1998) due to the fact that the chemistry of the hercynite synthesized here has a non-stoichiometric Fe:Al ratio of

0.43:1. As such, a single, derived order parameter based on Fe-Al distribution over *M* and *T* sites in our sample cannot be determined and would, regardless, be of limited relevance. Due to the fact that our hercynite sample is Fe-poor compared to the ideal, stoichiometric hercynite formula, a more useful expression of the degree of disorder is the amount of Fe present on the *M* site (^{M}Fe). The value refined from X-ray data, 0.126(5), is actually significantly higher than the value of ^{M}Fe = 0.112(4) in the most disordered sample of Harrison *et al.* (1998). Harrison *et al.* (1998) and Larsson *et al.* (1994) both note that high temperature disorder in synthetic hercynite cannot be quenched from above 900°C. Comparison of the degree of disorder noted here to that of synthetic hercynite at 900°C (Harrison *et al.*, 1998) implies that the extent of Fe-Al site mixing in our sample is significantly higher than expected, suggesting that disordering in hercynite is compositionally dependent. The extent to which Mn^{2+} and Mn^{3+} are disordered in our synthetic hercynite could not be determined due to limitations in data quality. Here we assume instead, consistent with previous studies, that Mn^{2+} and Mn^{3+} partition onto *T* and *M* sites, respectively. It can be hypothesized that either (1) extent of Fe-Al disorder in hercynite increases with a decrease in the ratio of Fe:Al, or, more likely, that (2) preferential incorporation of Mn^{2+} onto *T* sites and possibly also Mn^{3+} incorporation onto *M* sites increases the degree of Fe-Al disorder in hercynite. Lucchesi *et al.* (1997) note that preferential Mn incorporation onto *T* sites in Mn-rich spinels across the jacobsite ($MnFe_2O_4$)-franklinite ($ZnFe_2O_4$) solid solution results in changes in site distribution of Fe, with Fe^{3+} incorporation onto *M* sites enhanced. If present, Fe^{3+} would be expected to partition strongly onto the *M* site (e.g., Halenius *et al*., 2002; Lenaz *et al*., 2004, 2006), increasing the apparent degree of disorder in our hercynite. However, a significant fraction of Fe^{3+} would need to be present to explain the increased Fe-Al

disorder observed here which is unlikely due to the low fO_2 conditions imposed by the sample assembly. A similar influence of preferential partitioning of Mn^{2+} onto *T* sites provides the most obvious explanation for an effect of Mn content on Fe-Al partitioning in hercynite. Halenius *et al.* (2002) suggest that Al-deficiency in synthetic spinels could explain stabilization of Fe^{3+} defects on the *M* site, and therefore an apparent increase in the degree of Fe-Al disorder as expressed through *M* site occupancy. Therefore, it appears clear that the temperature dependence of ordering in hercynite derived from the studies of stoichiometric samples may be of limited applicability to more complex natural spinel compositions. Clearly, the compositional dependence of Fe-Al ordering in hercynite requires further study, especially if ordering is to be accurately used to constrain closure-temperatures in spinel-bearing rocks (Lavina *et al.*, 2009).

Comparison of hercynite and glass XANES spectra indicates that Mn^{2+} and Mn^{3+} partition preferentially into the glass and hercynite phase, respectively, at controlled *P-T-*fO_2. This, in combination with preferential partitioning of Mn^{2+} and Mn^{3+} onto spinel cation sites, suggests that Mn partitioning behavour might be used to determine fO_2 conditions in host magmas during crystallization of spinel. Under more reducing conditions, increase in the proportion of Mn^{2+} in magma would result in a lower Mn partition coefficient, $D_{spinel/melt}^{Mn}$, and a more Mn-poor hercynitic spinel with a higher proportion of tetrahedrally coordinated Mn, possibly also with a more ordered distribution of Fe-Al. In contrast, more oxidizing conditions and an increase in the proportion of Mn^{3+} would result in higher $D_{spinel/melt}^{Mn}$ and a more Mn-rich hercynitic spinel with a higher proportion of octahedrally coordinated Mn, and possible also a higher degree of Fe-Al disorder. Mn spinel-melt partitioning is likely to be influenced by a number of additional factors which would need to be accounted

for the development of an oxygeobarometer, most notably the effects of crystallization of other Mn-bearing phases such as biotite. However, the high temperature of crystallization of spinel might mean that the influence of co-crystallising phases is small, and that spinel retains an accurate measure of early magma fO_2 inherited from mantle source regions. Furthermore, degree of Fe-Al disorder in hercynitic spinels, once calibrated, could provide independent measure of closure temperature.

Ackowledgements

The authors thank Diamond Light Source for access to beamline i18 (SP9094), Konstantin Ignatyev for assistance with XANES measurement, and Chris Hayward for assistance with EMP analyses. GDG acknowledges the Italian Ministry of Education, MIUR-Project: 2010EARRRZ_003. The authors thank F. Camara and two anonymous reviewers for constructive comments.

References

Agilent. (2012) Xcalibur CCD system, Crysalis software system.

Andreozzi, G.B., Lucchesi, S., Skogby, H. and Della Giusta, A. (2001) Compositional dependence of cation distribution in some synthetic (Mg,zn)(Al,Fe^{3+})$_2O_4$ spinels. *European Journal of Mineralogy*, **13**, 391-402.

Andreozzi, G.B. and Lucchesi, S. (2002) Intersite distribution of Fe2+ and mg in the spinel (sensu stricto)-hercynite series by single-crystal x-ray diffraction. *American Mineralogist*, **87**, 1113-1120.

Anthony, J.W., Bideaux, R.A., Bladh, K.W. and Nichols, M.C. (1997) Handbook of mineralogy vol. III: Halides, hydroxides, oxides. Mineralogical Society of America, Chantilly, VA, USA.

Beard, J.S. and Tracy, R.J. (2002) Spinels and other oxides in Mn-rich rocks from the hutter mine, pittsylvania county, virginia, USA: Implications for miscibility and solvus relations among jacobsite, galaxite, and magnetite. *American Mineralogist*, **87**, 690-698.

Bosi, F., Halenius, U., Andreozzi, G.B., Skogby, H. and Lucchesi, S. (2007) Structural refinement and crystal chemistry of Mn-doped spinel: A case for tetrahedrally coordinated Mn^{3+} in an oxygen-based structure. *American Mineralogist*, **92**, 27-33.

Bromiley, G., Keppler, H., McCammon, C., Bromiley, F. and Jacobsen, S. (2004) Hydrogen solubility and speciation in natural, gem-quality Cr-diopside. *American Mineralogist*, **89**, 941-949.

Bromiley, G.D., Nestola, F., Redfern, S.A.T. and Zhang, M. (2010) Water incorporation in synthetic and natural $MgAl_2O_4$ spinel. *Geochimica Et Cosmochimica Acta*, **74**, 705-718.

Carbonin, S., Russo, U. and Della Giusta, A. (1996) Cation distribution in some natural spinels from X-ray diffraction and mossbauer spectroscopy. *Mineralogical Magazine*, **60**, 355-368.

Guillemet-Fritsch, S., Navrotsky, A., Tailhades, P., Coradin, H. and Wang, M. (2005) Thermochemistry of iron manganese oxide spinels. *Journal of Solid State Chemistry*, **178**, 106-113.

Halenius, U., Skogby, H. and Andreozzi, G.B. (2002) Influence of cation distribution on the optical absorption spectra of Fe^{3+}-bearing spinel s.s.-hercynite crystals: Evidence for electron transitions in $Fe^{VI}(2+)$-$Fe^{VI}(3+)$ clusters. *Physics and Chemistry of Minerals*, **29**, 319-330.

Harrison, R.J., Redfern, S.A.T. and O'Neill, H.S.C. (1998) The temperature dependence of the cation distribution in synthetic hercynite ($FeAl_2O_4$) from in-situ neutron structure refinements. *American Mineralogist*, **83**, 1092-1099.

Hill, R.J. (1984) X-ray-powder diffraction profile refinement of synthetic hercynite. *American Mineralogist*, **69**, 937-942.

Johnson, H.P. and Jensen, S.D. (1974) High-temperature oxidation of magnetite to maghemite. *Transactions-American Geophysical Union*, **55**, 233-233.

Kohn, S.C., Charnock, J.M., Henderson, C.M.B. and Greaves, G.N. (1990) The structural environments of trace-elements in dry and hydrous silicate-glasses - a manganese and strontium K-edge X-ray absorption spectroscopic study. *Contributions to Mineralogy and Petrology*, **105**, 359-368.

Larson, A.C. (1967) Inclusion of secondary extinction in least-squares calculations. *Acta Crystallographica*, **23**, 664-&.

Larsson, L., Oneill, H.S. and Annersten, H. (1994) Crystal-chemistry of synthetic hercynite ($FeAl_2O_4$) from XRD structural refinements and mossbauer-spectroscopy. *European Journal of Mineralogy*, **6**, 39-51.

Lavina, B., Cesare, B., Alvarez-Valero, A.M., Uchida, H., Downs, R.T., Koneva, A. and Dera, P. (2009) Closure temperatures of intracrystalline ordering in anatectic and metamorphic hercynite, $Fe^{2+}Al_2O_4$. *American Mineralogist*, **94**, 657-665.

Lavina, B., Princivalle, F. and Della Giusta, A. (2005) Controlled time-temperature oxidation reaction in a synthetic mg-hercynite. *Physics and Chemistry of Minerals*, **32**, 83-88.

Lenaz, D., Skogby, H., Princivalle, F. and Halenius, U. (2004) Structural changes and valence states in the $MgCr_2O_4$-$FeCr_2O_4$ solid solution series. *Physics and Chemistry of Minerals*, **31**, 633-642.

Lenaz, D., Skogby, H., Princivalle, F. and Halenius, U. (2006) The $MgCr_2O_4$-$MgFe_2O_4$ solid solution series: Effects of octahedrally coordinated Fe^{3+} on T-O bond lengths. *Physics and Chemistry of Minerals*, **33**, 465-474.

Liang, X.L., Zhong, Y.H., Tan, W., Zhu, J.X., Yuan, P., He, H.P. and Jiang, Z. (2013) The influence of substituting metals (Ti, V, Cr, Mn, Co and Ni) on the thermal stability of magnetite. *Journal of Thermal Analysis and Calorimetry*, **111**, 1317-1324.

Lotgering, F.K. (1964) Semiconduction + cation valencies in manganese ferrites. *Journal of Physics and Chemistry of Solids*, **25**, 95-&.

Lucchesi, S., Russo, U. and DellaGiusta, A. (1997) Crystal chemistry and cation distribution in some Mn-rich natural and synthetic spinels. *European Journal of Mineralogy*, **9**, 31-42.

Manceau, A., Marcus, M.A. and Grangeon, S. (2012) Determination of Mn valence states in mixed-valent manganates by xanes spectroscopy. *American Mineralogist*, **97**, 816-827.

Miles, A.J., Graham, C.M., Hawkesworth, C.J., Gillespie, M.R., Hinton, R.W. and Eimf. (2013) Evidence for distinct stages of magma history recorded by the compositions of accessory apatite and zircon. *Contributions to Mineralogy and Petrology*, **166**, 1-19.

Myers, J. and Eugster, H.P. (1983) The system Fe-Si-O -oxygen buffer calibrations to 1,500k. *Contributions to Mineralogy and Petrology*, **82**, 75-90.

O'Neill, H.S.C. and Navrotsky, A. (1983) Simple spinels - crystallographic parameters, cation radii, lattice energies, and cation distribution. *American Mineralogist*, **68**, 181-194.

Ravel, B. and Newville, M. (2005) Athena, artemis, hephaestus: Data analysis for X-ray absorption spectroscopy using ifeffit. *Journal of Synchrotron Radiation*, **12**, 537-541.

Raye, U., Anthony, E.Y., Stern, R.J., Kimura, J.I., Ren, M.H., Qing, C. and Tani, K. (2011) Composition of the mantle lithosphere beneath south-central laurentia: Evidence from peridotite xenoliths, knippa, texas. *Geosphere*, **7**, 710-723.

Redfern, S., Harrison, R., O'Neill, H.S.C. and Wood, D. (1999) Thermodynamics and kinetics of cation ordering in $MgAl_2O_4$ spinel up to 1600°C from in situ neutron diffraction. *American Mineralogist*, **84**, 299-310.

Righter, K., Sutton, S.R., Newville, M., Lei, L., Schwandt, C.S., Uchida, H., Lavina, B. and Downs, R.T. (2006) An experimental study of the oxidation state of vanadium in spinel and basaltic melt with implications for the origin of planetary basalt. *American Mineralogist*, **91**, 1643-1656.

Schollenbruch, K., Woodland, A.B. and Frost, D.J. (2010) The stability of hercynite at high pressures and temperatures. *Physics and Chemistry of Minerals*, **37**, 137-143.

Sheldrick, G. (1997) Shelx-97-a program for crystal structure refinement. Pp.,Institut fur Anorganische Chemie, University of Gottingen, Germany.

Turnock, A.C. and Eugster, H.P. (1962) Fe-al oxides - phase relationships below 1,000-degrees-c. *Journal of Petrology*, **3**, 533-565.

Wilson, A.J.C. and Prince, E. (1999) *International tables for x-ray crystallography, volume c: Mathematical, physical and chemical tables (2nd edition)*. Kluwer Academic, Dordrecht, NL.

Woodland, A.B. and Wood, B.J. (1990) The breakdown of hercynite at low fO_2. *American Mineralogist*, **75**, 1342-1348.

Table 1. Averaged compositions and oxide totals of hercynite (10 points analyses) and coexisting quenched silicate glass (8 point analyses) determined by electron microprobe[1].

phase	Na_2O	MgO	FeO[2]	Al_2O_3	SiO_2	K_2O	CaO	Cl	P_2O_5	SO_2	MnO	F	TOTAL[3]
Hercynite	0	1.14(14)	34.47(85)	57.22(68)	0.56(45)	n.d.	n.d.	n.d.	n.d.	n.d.	6.24(66)	n.d.	99.63(111)
Glass	3.44(10)	0.28(1)	17.65(84)	15.67(13)	39.67(73)	3.22(19)	10.60(9)	0.16(1)	0.81(3)	0.05(1)	6.90(24)	1.16(8)	99.41(90)

[1] Figures in parentheses are the standard deviations on the last significant figures of the average value, including oxide totals..

[2]All Fe assumed to be 2+ in accordance with the inherently low fO_2 conditions imparted by the sample assembly. See text for discussion. [3]Average of the oxide totals for all analyses.

Table 2. Averaged results of LCF of XANES data for hercynite and coexisting glass for proportion of each Mn oxidation state[1].

phase	2+	3+	4+
Hercynite	0.41(8)	0.53(7)	0.06(6)
Glass	0.72(14)	0.28(13)	-

[1] Figures in parentheses are 2σ errors on the last s.f. of each average value.

Table 3. Details pertaining the data collection and structural refinements of hercynite. Two refinements (left protocol 1, right protocol 2) were performed with different site populations (see text for further details).

Crystal size (μm^3)	150 x 130 x 90	
Radiation, detector type	Mo*K*α, CCD	
Scan type, width (°), time/frame (s)	ω, 1, 20	
Temperature (K), Pressure (bar)	293, 1	
Reference chemical formula, *Z*	$FeAl_2O_4$, 8	
Space group	$Fd\bar{3}m$	
a (Å)	8.1646(2)	
Calculated density (g/cm^3)	4.160	4.361
$2\theta_{max}$ (°)	71.5	
	-13 ≤ *h* ≤ 13	
	-13 ≤ *k* ≤ 13	
	-10 ≤ *l* ≤ 10	
No. collected reflections	3527	
No. unique reflections	84	
No. unique refl. with $F_o > 4\sigma(F_o)$	79	
No. refined parameters	10	
Extinction parameter	0.0086(8)	
R_{int}	0.0247	
R_1 *(F)* with $F_o > 4\sigma$ (F_o)	0.0115	0.0114
wR_2 (F^2)	0.0301	0.0298
GooF	1.427	1.414
Residual ρ_{max} / ρ_{min} (e^-/Å^3)	+0.26/-0.19	0.27/-0.19
T (8*a*), *x* =1/8		
Site population	$(Fe_{0.84(1)}Al_{0.16(1)})$	$(Fe_{0.77(1)}Al_{0.16(1)}Mn_{0.07})$
$^T\Sigma e$-	23.92	23.85
U_{11} (Å^2)	0.0075(2)	0.0075(2)
M (16*d*), *x* =1/2		
Site population	$(Al_{0.838(5)}Fe_{0.162(5)})$	$(Al_{0.834(5)}Fe_{0.126(5)}Mn_{0.040})$
$^M\Sigma e$-	15.11	15.12
U_{11} (Å^2)	0.0068(2)	0.0069(2)
U_{12} (Å^2)	-0.0005(1)	-0.0005(1)
O (32*e*), site population	$O_{1.0}$	$O_{1.0}$
x (u)	0.26375(9)	0.26375(9)
U_{11} (Å^2)	0.0104(3)	0.0104(3)
U_{12} (Å^2)	-0.0001(3)	-0.0001(3)
T-*O* (Å)	1.9621(13)	1.9621(13)
M-*O* (Å)	1.9354(7)	1.9354(7)

Note: origin fixed at $\bar{3}m$, $R_{int} = \Sigma \mid F_{obs}^2 - F_{obs}^2(mean) \mid / \Sigma [F_{obs}^2]$; $R_1(F) = \Sigma (|F_{obs}| - |F_{calc}|)/\Sigma|F_{obs}|$; wR_2 $(F^2) = [\Sigma [w(F^2_{obs} - F^2_{calc})^2] / \Sigma [w(F^2_{obs})^2]]^{0.5}$; s.o.f. are given as refined atomic fraction and as electron content per site Σe-. EMPA analysis shows the presence of Mg and Si (i.e., $Mg_{0.05(1)}$ and $Si_{0.02(1)}$ a.p.f.u.), ascribable to the population at the *T* site. It can be deduced that s.o.f.^{T}(Al + Mg + Si) = 0.16(1), with a resulting s.o.f.^{T}Al = 0.09(3).

The anisotropic displacement factor exponent takes the form: $-2\pi^2[(ha^*)^2U_{11} + \ldots + 2hka^*b^*U_{12} + \ldots + 2klb^*c^*U_{23}]$.

Figure captions

Figure 1. Normalised Mn *K* edge XANES spectra from natural Mn-bearing minerals (offset vertically for clarity). Green = rhodonite (octahedrally coordinated Mn^{2+}), blue = bixbiyite (octahedrally coordinated Mn^{3+}) and red = pyrolusite (octahedrally coordinated Mn^{4+}).

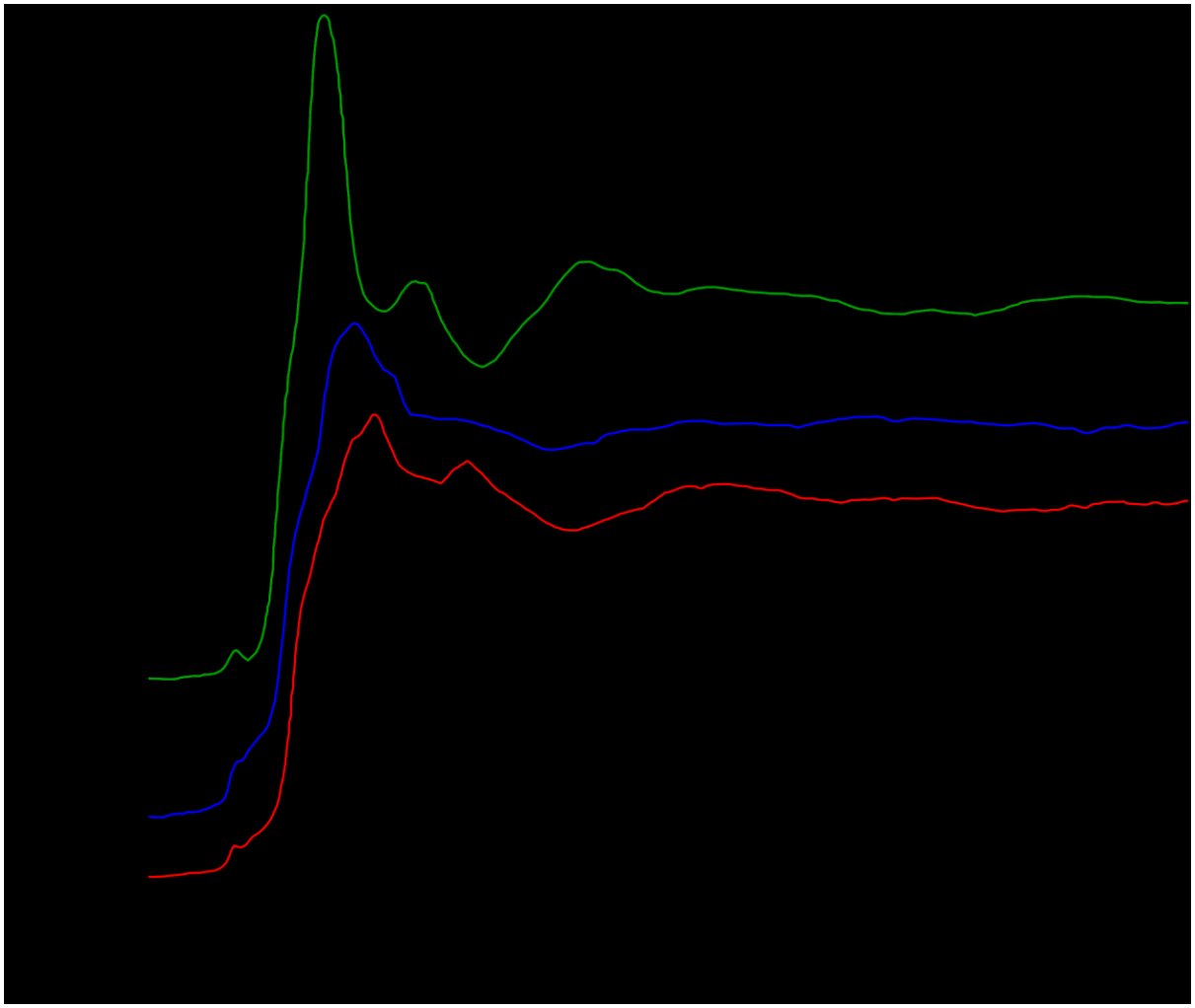

Figure 2. Normalised and background subtracted Mn *K* edge XANES spectra from synthetic hercynite (red) and coexisting silicate glass (blue).